

Effects of model error on cardiac electrical wave state reconstruction using data assimilation

Nicholas S. LaVigne, Nathan Holt, Matthew J. Hoffman, and Elizabeth M. Cherry

Citation: *Chaos* **27**, 093911 (2017); doi: 10.1063/1.4999603

View online: <http://dx.doi.org/10.1063/1.4999603>

View Table of Contents: <http://aip.scitation.org/toc/cha/27/9>

Published by the [American Institute of Physics](#)

Articles you may be interested in

[Modeling dynamics in diseased cardiac tissue: Impact of model choice](#)

Chaos: An Interdisciplinary Journal of Nonlinear Science **27**, 093909 (2017); 10.1063/1.4999605

[Memory in a fractional-order cardiomyocyte model alters properties of alternans and spontaneous activity](#)

Chaos: An Interdisciplinary Journal of Nonlinear Science **27**, 093904 (2017); 10.1063/1.4999351

[Slow \$\[Na^+\]_i\$ dynamics impacts arrhythmogenesis and spiral wave reentry in cardiac myocyte ionic model](#)

Chaos: An Interdisciplinary Journal of Nonlinear Science **27**, 093907 (2017); 10.1063/1.4999475

[Alternans promotion in cardiac electrophysiology models by delay differential equations](#)

Chaos: An Interdisciplinary Journal of Nonlinear Science **27**, 093915 (2017); 10.1063/1.4999471

[Distinguishing mechanisms for alternans in cardiac cells using constant-diastolic-interval pacing](#)

Chaos: An Interdisciplinary Journal of Nonlinear Science **27**, 093902 (2017); 10.1063/1.4999354

[Memory effects, transient growth, and wave breakup in a model of paced atrium](#)

Chaos: An Interdisciplinary Journal of Nonlinear Science **27**, 093917 (2017); 10.1063/1.4999601

Welcome to a

Smarter Search 

PHYSICS
TODAY

with the redesigned
Physics Today Buyer's Guide

Find the tools you're looking for today!

Effects of model error on cardiac electrical wave state reconstruction using data assimilation

Nicholas S. LaVigne,¹ Nathan Holt,² Matthew J. Hoffman,² and Elizabeth M. Cherry^{2,a)}

¹Center for Applied Mathematics, Cornell University, Ithaca, New York 14853, USA

²School of Mathematical Sciences, Rochester Institute of Technology, Rochester, New York 14623, USA

(Received 15 March 2017; accepted 7 July 2017; published online 24 August 2017)

Reentrant electrical scroll waves have been shown to underlie many cardiac arrhythmias, but the inability to observe locations away from the heart surfaces and the restriction of observations to only one or two state variables have made understanding arrhythmia mechanisms challenging. Recently, we showed that data assimilation from spatiotemporally sparse surrogate observations could be used to reconstruct a reliable time series of state estimates of reentrant cardiac electrical waves including unobserved variables in one and three spatial dimensions. However, real cardiac tissue is unlikely to be described accurately by mathematical models because of errors in model formulation and parameterization as well as intrinsic but poorly described spatial heterogeneity of electrophysiological properties in the heart. Here, we extend our previous work to assess how model error affects the accuracy of cardiac state estimates achieved using data assimilation with the Local Ensemble Transform Kalman Filter. We focus on one-dimensional states of discordant alternans characterized by significant wavelength oscillations. We demonstrate that data assimilation can provide high-quality estimates under a wide range of model error conditions, ranging from varying one or more parameter values to using an entirely different model to generate the truth state. We illustrate how multiplicative and additive inflation can be used to reduce error in the state estimates. Even when the truth state contains underlying spatial heterogeneity, we show that using a homogeneous model in the data assimilation algorithm can achieve good results. Overall, we find data assimilation to be a robust approach for reconstructing complex cardiac electrical states corresponding to arrhythmias even in the presence of model error. *Published by AIP Publishing.*

[<http://dx.doi.org/10.1063/1.4999603>]

Both experimental and simulated cardiac tissue readily supports scroll and spiral waves,^{1–6} which rotate at frequencies higher than the heart’s natural pacemaker and correspond to arrhythmic states. Lower-dimensional settings can support other complex dynamics, such as discordant alternans on ring geometries.^{7–9} However, reproducing these dynamics in a quantitative wave using a numerical model presents a number of challenges. Observations from experimental contexts typically are coarser in space and time than the resolution needed to resolve the dynamics numerically and generally can include observations only of voltage and perhaps intracellular calcium concentration, rather than the full complement of variables present in a model. Observations also may be restricted in other ways; for example, observations typically are limited to the surfaces of the heart when using the popular technique of optical mapping.^{10–12} Providing high-resolution, quantitatively accurate state reconstructions of the experiments may provide a clearer picture of the spatiotemporal dynamics underlying arrhythmias and perhaps lead to new mechanistic insights as well as potential improvements in model accuracy.

I. INTRODUCTION

Many arrhythmic states in the heart are characterized by the abnormal propagation of electrical waves. To provide better treatments, it is important to improve our understanding of the dynamics of these waves. Mathematical modeling can be a useful complement to traditional biological experiments by offering increased access to system variables and by providing additional levels of control over conditions. However, efforts toward developing reliable models that match experiments quantitatively are hindered in various ways, including limited locations for experimental recordings and restrictions to observe only one or a small number of variables, incomplete or inaccurate mathematical model formulation leading to a lack of quantitative agreement with experiments, and biological heterogeneity and variability that introduce further complications.

Recently¹³ we showed that data assimilation is a promising technique for reconstructing both observed and unobserved variables in a time series of cardiac electrical wave states from spatiotemporally coarse observations. Data assimilation arose in the weather-forecasting community as a way to use observations whenever and wherever they are available to improve predictions from imperfect and often sensitive numerical models. Essentially, the model is run until observational data, which are generally sparse in time as well as in space and are restricted to a subset of the model variables, are available, at which time they are used to

^{a)}Author to whom correspondence should be addressed: elizabeth.cherry@rit.edu

improve the model prediction. The approach can be used both for forecasting future states and for detailed reconstruction of past states, which is how we use it. Most data-assimilation methods, including ours, rely on the Kalman filter, which is a technique for producing state estimates from noisy data. We adopted an approach based on the Kalman filter called the Local Ensemble Transform Kalman Filter (LETKF).¹⁴ One of the main features of this method is that an ensemble of states is used to characterize uncertainty of the numerical prediction model, which affects how much weight the algorithm places on the observations in comparison with the numerical prediction when updating the state estimate at times when observational data are available.

The LETKF has been shown to be effective for atmospheric^{15–19} and oceanographic²⁰ applications. Within settings more closely related to the heart, Kalman filters have been used for state estimation in single cardiac cells²¹ and one-dimensional fibers.²² Berg *et al.*²³ considered a type of data assimilation in a setting more similar to our previous and present work by studying under what conditions a two-dimensional system with spiral-wave dynamics could be used to drive and synchronize a paired system through feedback. Data assimilation also has been used in other biological contexts to reconstruct the dynamics of networks of neurons during seizures,²⁴ to identify effective connections between spinal cord neurons in culture,²⁵ and to improve numerical model forecasts of the spread of brain cancer.²⁶

It is clear that the accuracy of the state estimates data assimilation provided will be limited by how well the numerical model used within the process represents the true dynamics of the system. We anticipate a number of possible problems that can arise: inaccurate (or highly sensitive) model parameter values, missing or incorrect model terms, differences among experimental preparations, and intrinsic spatial heterogeneity of electrophysiological properties, to name a few. In our previous work,¹³ we considered a single model-error case by using synthetic observations generated from a model to show that changing one parameter value between the model used for the truth and the model used for the reconstruction could be managed successfully by the LETKF.

This paper extends our previous work to consider a much broader range of cases of model error. First, we consider cases when the same model is used to generate the truth as is used in the LETKF and a single sensitive parameter is varied over a broad range of values. Next, we vary the values of multiple parameters that cause significant dynamics changes within the model used to generate the truth, which remains the same as that used in the LETKF. Then, we use a different numerical model to generate the truth and assess how well the LETKF can reconstruct truth states with different dynamics. Finally, we study a preliminary case in which the truth model includes spatial heterogeneity in a single parameter. We find that data assimilation can be used with high accuracy to construct high-resolution estimates of observed and unobserved variables under a broad range of conditions, including significant differences in dynamics between the truth state and the intrinsic behavior

of the model used within the LETKF to generate the reconstruction.

II. METHODS

A. Data assimilation

We adhere closely to the data-assimilation methodology outlined in our previous work,¹³ so we will provide only a brief description here. Essentially, data-assimilation schemes are used to generate improved state estimates for a system by combining observational data with numerical model predictions, which in turn have been informed by older observations. In this case, we form a state reconstruction; data assimilation also can be used to develop a prediction. We use the Local Ensemble Transform Kalman Filter (LETKF),¹⁴ which is a nonlinear extension to the Kalman filter. Observational data (with noise) are used to iteratively update a state estimate generated from a numerical model (we will refer to this initial estimate as the model prediction); here, we use a fixed assimilation interval. An improved state estimate is generated by minimizing a cost function that includes terms representing how close the improved estimate is to the available observations (which may be sparse in space and which may not include all state variables in the numerical model) and to the prediction from the numerical model. The algorithm weighs these terms dynamically by their covariances.

Rather than forming and inverting a large covariance matrix, the LETKF uses an ensemble of states to characterize uncertainty in the numerical prediction. The basic idea is that the more numerical-model solutions starting from slight perturbations of initial conditions (representing a state estimate) diverge by the time additional observations are available for assimilation, the more strongly the algorithm weighs the observations during assimilation. A single initial prediction from the numerical model is calculated at the end of each assimilation interval by averaging the solutions of the individual ensemble members obtained by running the numerical model for each perturbed initial condition over the time interval. The LETKF then combines the observations, numerical prediction, observation covariance, and ensemble sample covariance to produce an updated state estimate and a set of perturbations used to form the new ensemble members, and the process is repeated. To reduce the risk of spurious correlations over long distances, the LETKF is localized in the sense that only observations within a prescribed distance are considered when assimilating data for each grid point. More details and key equations are given in the [Appendixes A and B](#) and in Ref. 13.

In our case, we use an ensemble with 20 members, which was shown previously¹³ to be sufficient for characterizing uncertainty in our application. Each ensemble member is initialized to a randomly selected state of the numerical model from a 1000-ms spinup run. For numerical prediction, we use the Fenton-Karma model, as discussed below. Within the model, the time step is set to 0.05 ms and the spatial resolution is 0.025 cm. We set the spatial localization parameter value to 0.05 cm, so that approximately six observations are used to update the state estimate for each grid point.

To understand the performance of our algorithm in the presence of model error, we create synthetic observations from truth states generated from models. In all cases, truth states are generated as propagating waves on one-dimensional ring geometries 13.5 cm long. To create observations, we first subsample the truth voltage variable in space and time to a resolution of 0.075 cm in space and 5 ms in time (every 3 spatial grid points and 100 time steps of the numerical model). These values are consistent with resolutions available using optical mapping.²⁷ Then, we add Gaussian error with a mean of zero and standard deviation of 0.05. The resulting data are the observations used by the algorithm to reconstruct the truth state.

Because of the relatively small number of ensemble members used, ensemble Kalman filters frequently underestimate the covariance associated with the numerical prediction. A common strategy to compensate for this underestimation is the use of multiplicative inflation,^{14,16,18} which involves simply multiplying the covariance by a fixed constant factor m . When no multiplicative inflation is used, $m = 1$. In the cases studied here, we use $m = 1.2$ unless noted otherwise. In most cases, we also employ an additional strategy, additive inflation,^{18,19} which can modify the subspace spanned by the ensemble members by adding a vector to each ensemble member. Additive inflation is helpful for providing new directions to the ensemble when the error and ensemble subspaces do not coincide. Following our previous work,¹³ we use additive inflation vectors obtained as the difference between model states obtained in the spinup that are 5 ms (the assimilation interval) apart, scaled by a factor $a = 0.05$ unless noted otherwise. When additive inflation is not used, $a = 0$. More details are given in the [Appendixes A and B](#).

B. Cardiac models

We use two different cardiac models in this work. The Fenton-Karma (FK) model^{6,28} is always the numerical prediction model employed by the LETKF and in many cases also is used to generate the truth states we aim to recover through data assimilation. We use the Fenton-Karma model because it has been shown previously to be an efficient and flexible model that can reproduce many types of dynamics.^{6,29–32} Thus, we expect it to be useful for state reconstruction in a wide variety of settings.

The model consists of three variables, u , v , and w , and three currents (fast inward, slow inward, and slow outward). Here, the variable u represents the voltage, v is an inactivation variable for the fast inward current, and w is an inactivation variable for the slow inward current. A total of 13 parameters are used in the model. The model equations and parameter values used are given in [Appendixes A and B](#). Specific parameters considered here include τ_d , which represents excitability and affects wave speed and alternans magnitude; τ_r , which is the magnitude of the early repolarizing current and affects wavelength and alternans magnitude; and τ_{si} , which scales the slow inward current and also affects wavelength and alternans magnitude.

The numerical prediction model within the LETKF always uses the parameterization of the model tuned to

match action potential durations, but not action potential shapes, of the Beeler-Reuter (BR) model,³³ given as Set 3 in Ref. 6 and referred to here as the BR parameter set. We use resolutions of 0.025 cm and 0.05 ms in space and time, respectively. The geometry is a one-dimensional ring that is 13.5 cm long. For the BR parameter set, in this ring size the model generates a discordant alternans state characterized by pronounced oscillations in wavelength.

Truth states in some cases, as noted, are generated using the BR model,³³ which in its default configuration also results in discordant alternans for the ring size of 13.5 cm that we use in all cases. We also varied the parameter g_{Na} , which is the conductance of the sodium current. Increased g_{Na} leads to faster wave propagation and enhanced alternans; decreased g_{Na} slows propagation and reduces the magnitude of alternans.

C. Error metrics

To quantify the accuracy of the state estimates produced, we use three different error measurements. First, we use the standard root mean square (RMS) error, which is obtained by summing the squares of the pointwise differences between two vectors, taking their mean by dividing by the length of the vectors, and then taking the square root. We use RMS to compare the reconstructed voltage with the true voltage. The reconstructed voltage ideally will be within the observation error of the truth, and reduction of the RMS error over time is positive. Because RMS error in the present case is sensitive to differences in waveforms, which can vary significantly between different model parameterizations or between different models, we also consider in some cases what we call a binary error metric, which is the fraction of all estimated values of u that are incorrectly above or below a threshold of 0.1 compared to the truth. This metric is sensitive along the wave fronts and backs but is more forgiving of differences in waveforms within the interior of the wave. Finally, we also measure the wavelength over time using a threshold of 0.15. We consider both the average wavelength measured across all times and the extreme wavelength values reached in the second half of the simulation, as noted.

III. RESULTS

A. No model error

As a first demonstration of the data-assimilation algorithm and our setup, we consider a case with no model error. Figure 1 shows a space-time plot of the truth (upper left), which is a simulation of discordant alternans on a ring geometry using the FK model with the BR parameter set, along with representative wave profiles at different times (upper right). Observations are generated from a subsampling of the truth with the addition of Gaussian noise and random model states are used to initiate the 20 ensemble members, as described in the Methods. For this first case, no inflation is used ($m = 1$, $a = 0$). The estimate achieved by the LETKF is shown in the lower left of Fig. 1. Early on, the reconstructed state estimate has trouble achieving resting membrane potential (lighter blue color following some waves). However, within two rotations

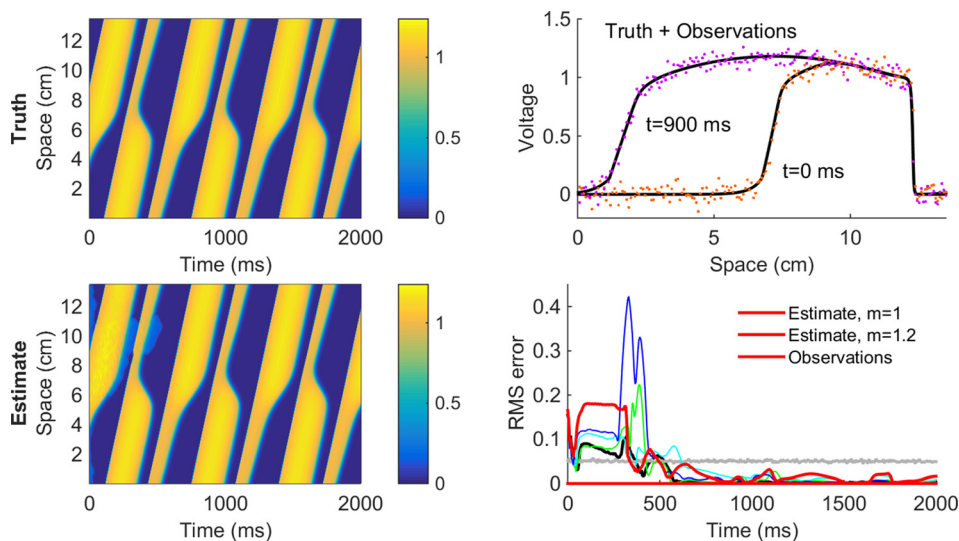


FIG. 1. An example with no model error. Here, the LETKF is run using the FK model with the BR parameterization to generate the truth and to reconstruct the estimate from synthetic observations. No inflation is used ($m = 1$, $a = 0$) except where noted otherwise. The truth state (top left) shows discordant alternans and can be compared to the estimate (bottom left). Two spatial voltage profiles taken at different times from the truth (top right) demonstrate the change in wavelength characteristic of the discordant alternans state (profiles were shifted spatially to aid visualization); scattered points below the level of noise in the observations, but does not go to zero for multiplicative inflation factor $m = 1$. Setting $m = 1.2$ improves the estimate and results in the black RMS error plot. The randomness involved in selection of the initial ensemble leads to different estimates; the RMS error plot includes the error values of the estimates obtained from three other simulations using $m = 1$ in green, cyan, and blue, corresponding to the other estimates shown in Fig. 2.

around the ring, which roughly corresponds to one discordant alternans period, the RMS error has dropped below the level of the added Gaussian noise (standard deviation of 0.05, gray), as seen in the RMS error plot (lower right, red).

It is important to keep in mind that the initialization of the model to random states introduces a stochastic component to the LETKF that can affect its performance somewhat. The blue, green, and cyan traces in the error plot in Fig. 1 show how RMS error changes for three other initializations with all model and algorithmic parameters unchanged. All drop below the noise level within roughly the same amount of time, but some reach higher levels of error than others. Figure 2 shows the space-time plots of the estimates resulting from these repetitions along with space-time plots of the difference from the truth. The top row shows the same estimate as Fig. 1 but includes the difference plot as well. The main sources of error are the inability to achieve resting membrane potential in some regions early over the first several hundred ms, as evidenced by the red regions indicating an overestimate of the voltage, and some early underestimation of the voltage along the wave front, which could have led to a lag in the wave if not for the correcting influence of the observations. Although the RMS error overall drops below the level of noise in the observations, the difference plot shows continued regions with overestimation and underestimations of the voltage.

The different initializations with $m = 1$ show similar behavior but include some differences. Notably, in one case there is a wave break that heals quickly, and in another there is a pronounced wave break that temporarily leads to a bidirectionally propagating wave. All of the simulations share early difficulties in achieving resting membrane potential (overestimates of voltage, red) and in matching the wave front location exactly (underestimates of voltage, blue). However, the assimilation of observations corrects even the most

egregious cases and reduces the error to a low value. Nevertheless, most of the cases show small but observable deviations from the truth throughout the 2-s simulations, as shown in the continued presence of light red and blue regions in the difference plots. Note that these regions are concentrated around the wave fronts and backs, which also are the locations with the sharpest spatial gradients, so they are the most sensitive to differences and the most challenging to estimate accurately.

The reason for persistent differences is a phenomenon called ensemble collapse, which we also observed in our previous work.¹³ Essentially, the ensemble members become very similar, leading to a low covariance and high confidence in the numerical model prediction. Thus, the LETKF places more weight on the model prediction and less on the observations during the assimilation steps. This situation can arise readily because of the small ensemble, which can lead to an underestimate of the covariance for the numerical prediction. One approach for reducing the likelihood of ensemble collapse is to use multiplicative inflation to artificially increase the covariance. This strategy works well in this case: setting multiplicative inflation to $m = 1.2$ improves the estimate, as can be seen in the plot in the last row of Fig. 2 as well as the black error plot in Fig. 1. Now the RMS error approaches zero, and the difference plot does not show any noticeable discrepancy between the estimate and the truth after about the first 500 ms.

B. Model error: Changing a single parameter value

The case with no model error just considered provides a proof of concept for data assimilation in cardiac models, but in reality we would expect that the model used in the LETKF would not describe the dynamics of the truth state

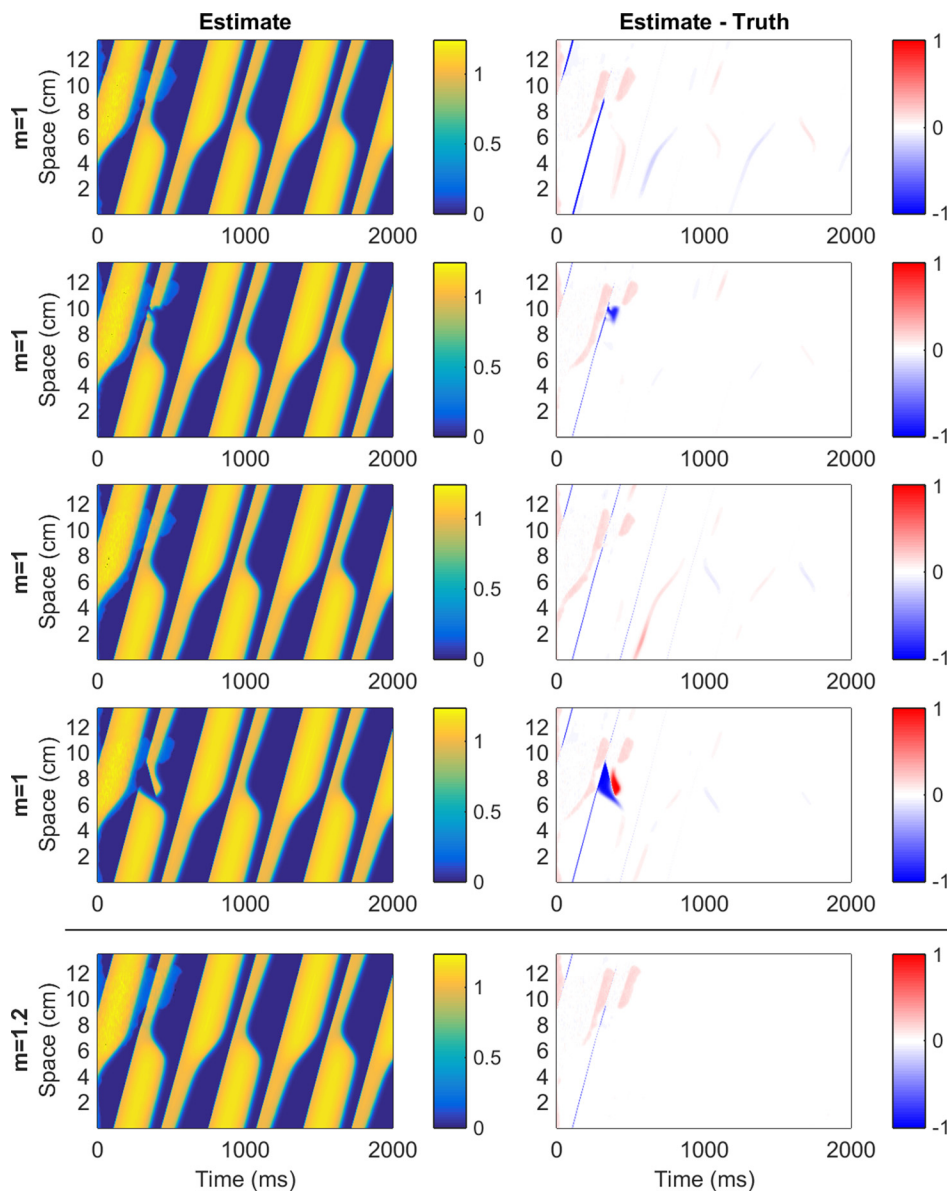


FIG. 2. Variability in estimates with no model error. Although all estimates shown are based on the truth state shown in Fig. 1, variability due to the random selection of states used to initialize the ensemble leads to differences in the estimate for different runs of the LETKF. The top row shows the same case as Fig. 1, and the next three rows show three other reconstructions found using the same model and algorithm settings. The left column shows space-time plots of the estimate and the right column shows space-time plots of the difference between the estimate and the truth. The bottom row shows a single case with multiplicative inflation set to $m = 1.2$, which improves the estimate. The RMS error plots for all these cases are shown (in order from top to bottom) in red, green, cyan, blue, and black in Fig. 1.

with complete fidelity. Many factors can contribute to differences between the truth and the model, including incorrect model parameter values, missing or inaccurate model terms, biological variability, and errors in the approximations used to solve the model.

We first consider a case where a single parameter value is changed; later, we will introduce more variations. We select τ_d as the parameter to modify initially because of its strong effects: it plays the role of an excitability parameter and thus influences the magnitude of alternans as well as the wave speed. Figure 3 shows the truth state obtained when $\tau_d = 0.29$. The increased value leads to a reduction in wave speed (which can be verified visually through comparison with the truth space-time plot in Fig. 1) as well as a significant decrease in alternans magnitude. The numerical prediction model used by the LETKF keeps τ_d set to 0.25, which in the absence of data assimilation would match the dynamics of the truth state in Fig. 1.

Figure 3 shows what happens in this case with no inflation used ($m = 1$, $a = 0$). The algorithm initially can find the correct wave front location and wavelength (top right), but

over time discrepancies grow (center right) because the algorithm model parameters result in a faster wave with more prominent alternans. The main problem early on is that the algorithm is not fitting the resting membrane potential, but soon the error grows again as the assimilation overestimates the wave speed and consequently goes out of phase with the truth. In addition, the estimate overstates the degree of alternans. Thus, the RMS error grows beyond the noise level despite a low error initially (Fig. 3, lower right).

As in the case without model error, the inclusion of multiplicative inflation is helpful in mitigating the discrepancies between the estimate and the truth. When multiplicative inflation is introduced by setting $m = 1.2$, the maximum RMS error is much lower, as shown in Fig. 4 (cyan, compared with red for $m = 1$). Increasing the multiplicative inflation factor further can yield further reductions in error, but eventually it can grow too large and cause the error to increase. For the case we consider, the minimum error seems to be reached for $m \approx 1.6$ (blue). Similar results can be obtained when m is kept at a more modest value of 1.2 by

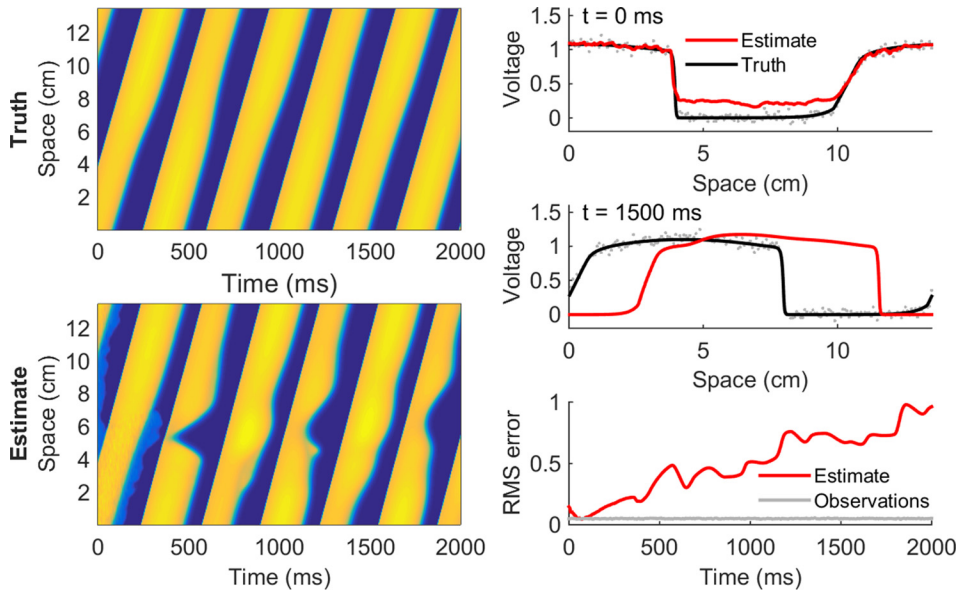


FIG. 3. Results from changing one parameter used to generate the truth state with no inflation. In the truth FK model $\tau_d = 0.29$ and in the forecasting FK model $\tau_d = 0.25$. The alternans in the truth state is now greatly reduced and the propagation speed of the wave is also decreased. Initially, the estimate and the truth align well, with the main problem being difficulty in achieving resting membrane potential in the estimate. However, the error grows over time (center right) because the wave in the estimate travels faster and exhibits more pronounced alternans. Therefore, the RMS error grows with time despite a low error initially (bottom right). Wave profiles include synthetic observations as gray dots.

introducing additive error as described in Sec. II. When $a = 0.05$, the error for the $m = 1.2$ case (black) is essentially at the minimum level achievable through multiplicative inflation alone and is basically at the level of noise present in the observations. Figure 5 shows space-time plots and space-time difference plots, including errors in the unobserved model variables, for the three cases $m = 1$, $m = 1.2$, and $m = 1.2$ with $a = 0.05$ from Fig. 4. When $m = 1$, the wave propagates too quickly and produces more significant alternans, leading to growing differences from the truth. Setting $m = 1.2$ decreases but does not eliminate differences. Including additive inflation further improves the estimate and decreases the difference from the truth. Note that a slight overestimate of the voltage remains along the leading edge of the wave (as also can be seen in the error plot for the unobserved variable v , which is the voltage-dependent inactivation gating variable regulating the fast inward current), but

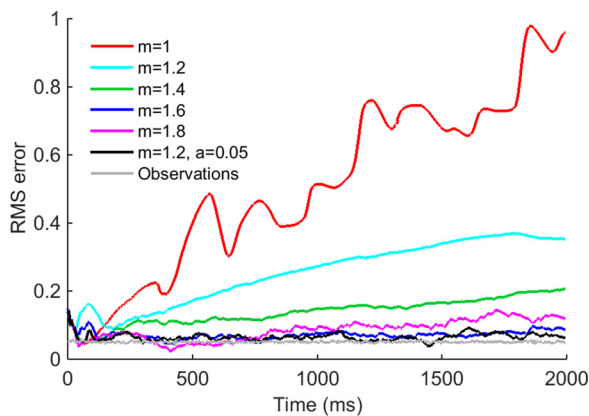


FIG. 4. RMS error in the model error case shown in Fig. 3. for different inflation values. With no multiplicative or additive inflation (red), the error grows throughout the time simulated, corresponding to the space-time plot in Fig. 3. When multiplicative inflation is used alone, as the multiplicative inflation factor m is increased, the RMS error after 2 s initially decreases and then increases, with the lowest error occurring for $m = 1.6$ (blue). Using additive inflation can decrease error further: using $m = 1.2$ in conjunction with an additive inflation factor of $a = 0.05$ (black) reduces the error by more than a factor of 5 compared to when $a = 0$.

regular incorporation of observations now keeps the error in check by correcting the voltage quickly and preventing error growth. In general, we found that using additive inflation gave more robust results, so for the remaining cases we discuss we set $a = 0.05$ along with $m = 1.2$.

To obtain a broader understanding of the role of model error in the quality of reconstructed state estimates from data assimilation, we considered varying a single parameter over a range of values when generating the truth state (and, correspondingly, the observations used for assimilation). Specifically, we quantified the accuracy of solutions obtained when separately varying τ_d between 0.21 and 0.29 and τ_r between 27 and 33.66. The parameter τ_r essentially sets the speed of repolarization, with smaller values associated with a larger repolarization current and therefore shorter action potentials and decreased alternans. Figure 6 shows two different error metrics. The top row shows the RMS error averaged over all simulation times. For τ_d , the RMS error in the voltage is below the level of noise in the observations for most of the values within the range tested, with slightly increased values at the extremes. For τ_r , the error was fairly low across the full range of values tested but was slightly higher for lower values of τ_r .

We also measured the average wavelength across all times as well as the maximum and minimum wavelengths obtained during the second half of the 2-second simulations. For the simulations varying τ_d in the truth, only very slight differences can be seen. When τ_r is varied in the truth, very good agreement is seen over most of the range, with only small overestimates of the wavelength for small values of τ_r when wavelengths are short and no alternans is present. Noise present in the observations reduces the quality of the wavelength measurements using those data; lower thresholds for wavelength measurements prevent the use of lower thresholds, although such lower thresholds can be used for obtaining wavelength measurements from the truth and from the estimate.

C. Model error: Changing multiple parameter values

The model parameters we studied when varying a single parameter have significant effects on dynamics, including

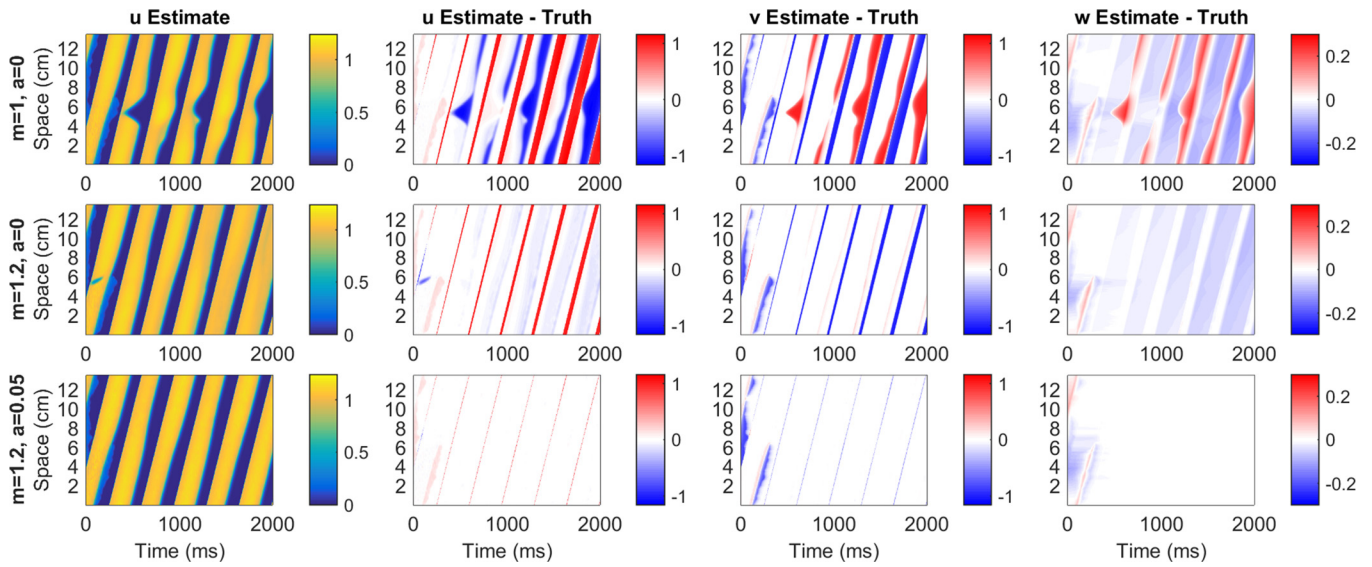


FIG. 5. Space-time plots of the state estimate and difference from the truth in the model error case from Fig. 3 with different inflation values; errors in the unobserved variables v and w are included. The top row shows the same case as Fig. 3, with no inflation ($m = 1, a = 0$). The RMS error grows over time as the estimated state diverges from the truth. The middle row shows an improvement when multiplicative inflation is used ($m = 1.2$; cyan RMS plot in Fig. 4). The bottom row shows further improvement in the estimate and a corresponding decrease in the difference from the truth with the inclusion of additive inflation ($a = 0.05$; also see the black RMS plot in Fig. 4).

wave speed, wavelength, and degree of alternans, and our data assimilation approach performed well under most conditions. To ensure that there was no advantage in having to overcome only a single incorrect parameter value, we next considered cases where multiple parameter values were different between the truth state and the numerical prediction model. First, we looked at changing combinations of the two parameters we varied separately before, τ_d and τ_r . Figure 7 shows estimates obtained for truth states generated using three different combinations of values for these two parameters. The truth states showed a wide variety of dynamics. For

a case with alternans similar to what the numerical prediction model would generate on its own but with faster propagation (Fig. 7, top row), the estimate has slight difficulties early in the simulation reaching resting membrane potential and sustaining propagation, but it adapts quickly; in less than 500 ms the RMS error for all variables (including unobserved v and w) drops below the level of noise added in generating the observations. In another case, the truth exhibited reduced alternans with slower propagation (Fig. 7, middle row). Although the parameter values of the LETKF on their own would produce faster propagation with prominent alternans,

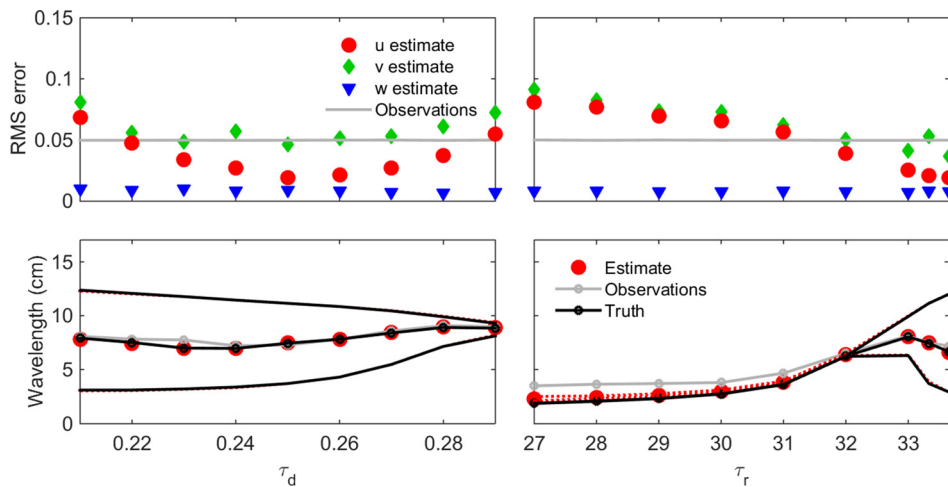


FIG. 6. Effectiveness of the LETKF when the value of one parameter in the truth state is varied over a wide range. The parameter τ_d , which is set to 0.25 in the LETKF, is varied from 0.21 to 0.29 (lower values are associated with faster propagation and more pronounced alternans; for even lower values, propagation is blocked for this ring size). The parameter τ_r , which is set to 33.33 in the LETKF, is varied from 27 to 33.66 (larger values are associated with increased wavelength and more pronounced alternans; for even larger values of τ_r , propagation fails). The top row shows RMS error for all three variables; the mean of the Gaussian error added when creating surrogate observations is shown for comparison. The bottom row shows the average wavelength measured across all times using a threshold of 0.15. Lines without markers indicate the maximum and minimum values of the wavelength measured over the last second for both the truth and the estimate. Maximum and minimum values for wavelengths calculated directly from the observations are not shown because the effects of noise significantly degrade these measurements.

the corrections provided by the observations allow the algorithm to converge to the truth with a low RMS value for all variables within about 400 ms.

The algorithm has a more difficult time handling a third case, which has stronger alternans combined with slower propagation (Fig. 7, bottom row), especially with finishing short waves on time. However, with a slight delay the LETKF is able to recover from the short waves, which are not supported in its model configuration, and the RMS error in u overall oscillates around the level of noise in the observations. The RMS error for v is higher with more frequent spikes corresponding to an inability to reset quickly following a wave (because of the more severe alternans in the truth caused by the elevated τ_r), but it does not grow over time; in contrast, the error in w is minimal.

We also studied cases where we varied even more parameters, following other published parameterizations of the FK model, as shown in Fig. 8. One parameter set (labeled “Traj”) we used was from Ref. 6, where it was referred to as parameter set 1 and was used as the basis for generating many different spiral wave trajectories in two dimensions. In a 13.5-cm ring, this parameter set produces waves with no alternans but a propagation speed similar to that of the BR parameter set used in the numerical prediction model. Although the BR parameter set would produce alternans on its own, through regular assimilation of observations it is able to match the dynamics of the truth state, and RMS error in all variables drops below the level of noise in the observations within 300 ms. We also generated a variation of the “Traj” parameter set that produced alternans; we refer to this as the “Alt Traj” parameter set. When the “Alt Traj” parameter set is used, the LETKF is able to adjust well, with the average RMS error in all variables approximately the same as the level of noise in the observations, except for spikes coinciding with a collapse in the wave back associated with discordant alternans in which three wave backs are transiently present in the ring.

As another example, we developed a modification of the guinea pig parameter set from Ref. 28 that produced alternans coupled with fast wave propagation and shorter average wavelengths. For this “Alt GP” parameter set, the data-assimilation algorithm has a difficult time matching the dynamics. In particular, matching the fast wave speed is problematic. The estimate shows jagged wave fronts where it repeatedly lags behind, and then catches up with, the truth. An important note is that although the error is not low, it did not grow without bound. When the parameter set is further modified to slow propagation by doubling τ_d , resulting in the “Slow Alt GP” parameter set, the LETKF is much better able to match the dynamics, and the average value of RMS error in u is approximately at the level of noise in the observations.

D. Model error: Using a different model for the truth

As a more significant model error case, we also considered using another model to generate the truth state. We chose the BR model, which generates alternans readily. In addition, a good parameterization of the FK model to match action potential durations over a broad range of cycle lengths already existed, which could serve as the best case to use in the numerical prediction algorithm. Using the BR model to generate the truth introduced another step in generating observations, because the FK model is “semi-normalized” (the action potential upstroke, but not the full action potential, is scaled between 0 and 1). Thus, we shifted and rescaled voltages from the BR model, which are in physical units of mV, to fall between 0 and 1.6 before generating observations for use with the LETKF.

Once the observations were generated, we found that the data-assimilation algorithm produced an estimate that in many ways agreed well with the truth state, as shown in the top row of Fig. 9. Although the action potential shape is very different for the BR model compared to the FK model even

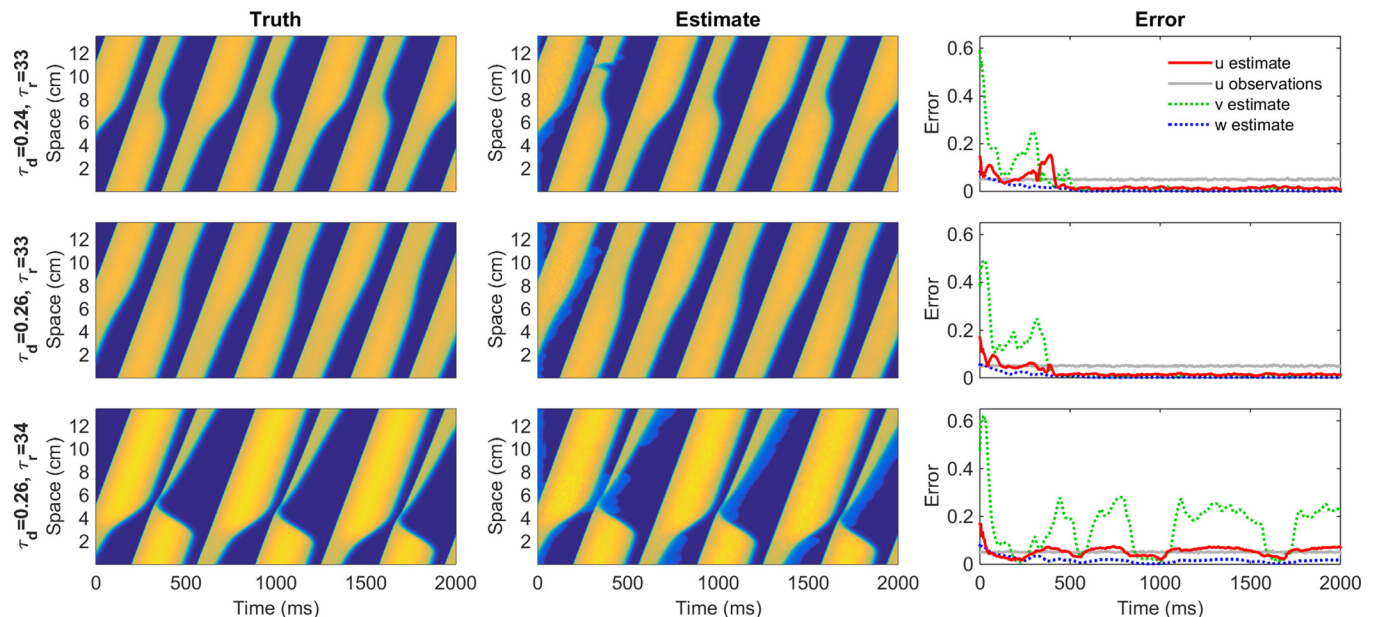


FIG. 7. Effectiveness of the LETKF when the values of two parameters in the model used to generate the truth state are varied simultaneously to test a variety of different dynamical states. Top row: $\tau_d = 0.24$ and $\tau_r = 33$. Middle row: $\tau_d = 0.26$ and $\tau_r = 33$. Bottom row: $\tau_d = 0.26$ and $\tau_r = 34$.

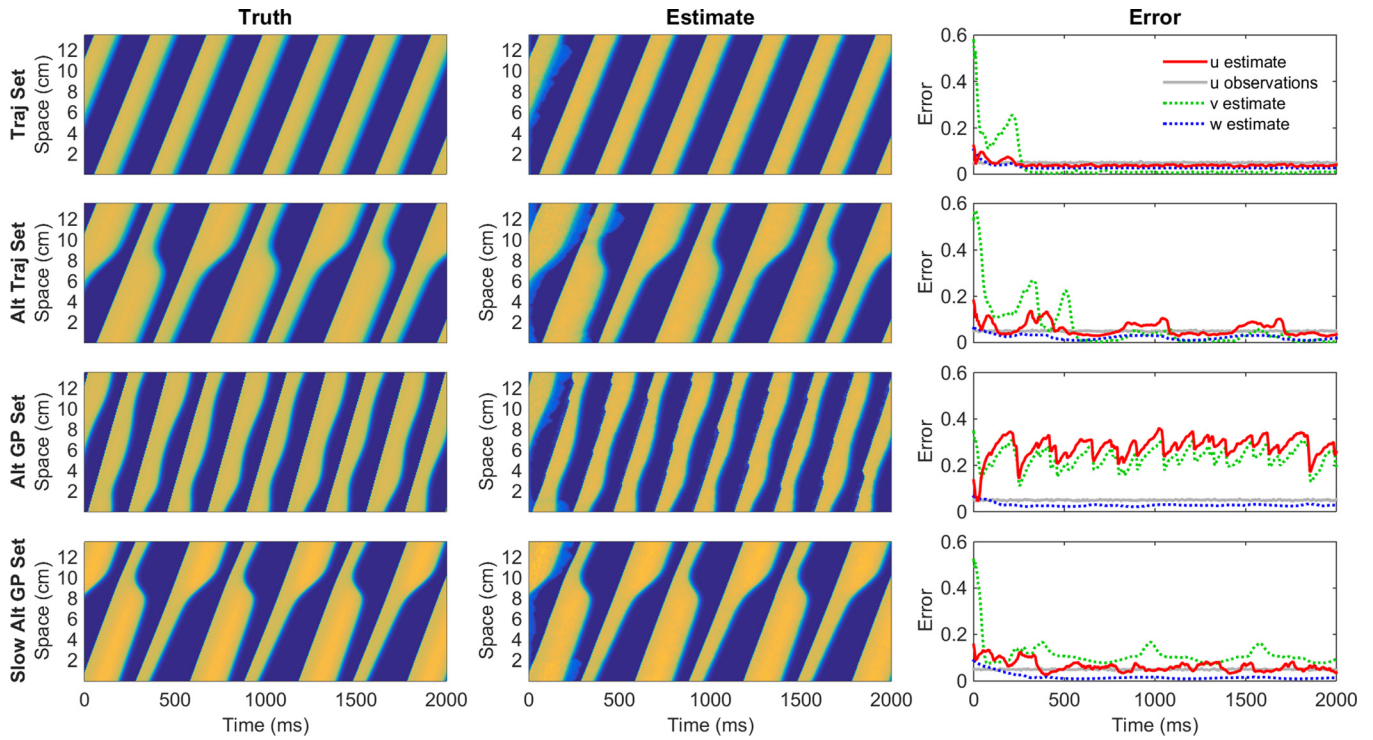


FIG. 8. Effectiveness of the LETKF when the values of many parameters used in generating the truth state are varied simultaneously based on previously published parameter sets, while the algorithm continues to use the BR parameter set. Top row: “Traj” parameter set. Second row: “Alt Traj” parameter set. Third row: “Alt GP” parameter set. Bottom row: “Slow Alt GP” parameter set. Parameter values are given in the [Appendixes A and B](#).

with the BR parameter set, as can be seen in the wave profile, the LETKF is able to match the overall wave pattern.

We also tested cases where we varied the parameter g_{Na} in generating the truth state; increasing (decreasing) g_{Na} increases (decreases) wave speed and alternans intensity. Thus, the numerical prediction model within the LETKF no longer was matched to the dynamics of the truth state. Nevertheless, the estimates produced in both cases essentially were as accurate as those where the numerical prediction model matched the truth model more closely. For all the cases, the RMS error values (which are calculated only for the voltage because of the differences in the FK and BR model formulations) remain high because of discrepancies in

the action potential shape, including the plateau height. In comparison, the binary error in the voltage decreases to the level of the binary error in the observations, with periodic spikes that coincide with the times when the wavelength transitions from long to short, which causes the wave to collapse in the middle and transiently develop two additional wave backs.

E. Model error: Spatial heterogeneity in the truth

Reconstructing states from real cardiac tissue poses challenges beyond limitations of the model used to describe it. In particular, cardiac tissue is not spatially homogeneous:

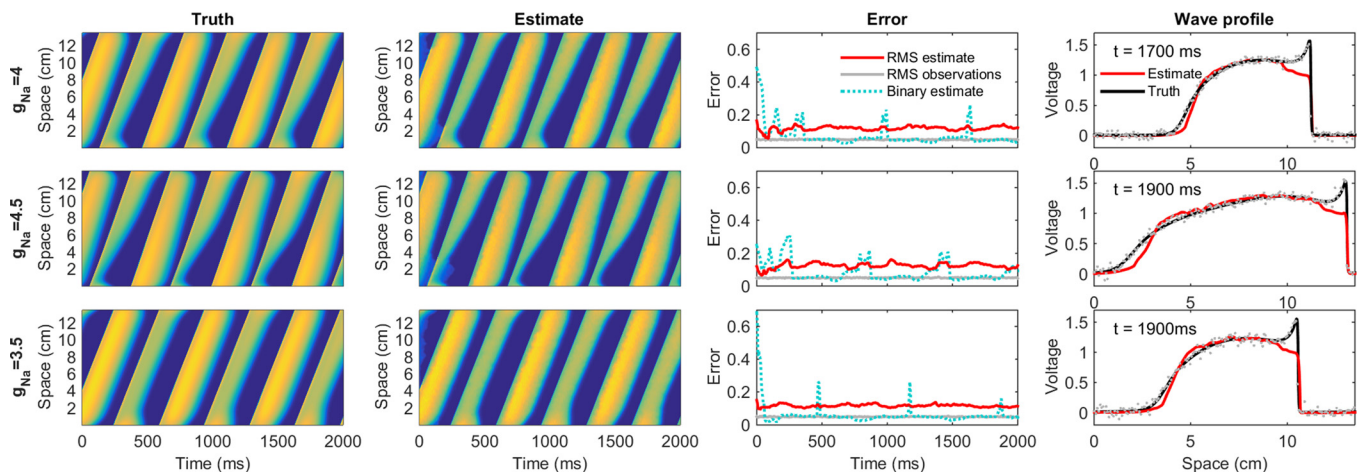


FIG. 9. Effectiveness of the LETKF when a different model, in this case the Beeler-Reuter model, is used to generate the truth state. The top row shows results from using the original model with $g_{Na} = 4$ and the lower rows show results obtained when g_{Na} is set to 4.5 and 3.5, which increase and decrease the wave speed and alternans magnitudes, respectively. Gray dots in the wave profiles indicate the synthetic observations.

different parts of the tissue, including transmural, left-right, apex-base, and anterior-posterior, can have different electrophysiological properties, primarily because of differences in ion channel expression. Although some spatial gradients have been described,^{34–38} the precise details of the heterogeneity typically vary among experiments and may be difficult to specify. Because data assimilation allows localized corrections based on observations, we expected that it could perform well even in a setting with spatial heterogeneity.

We tested the LETKF for a case where the underlying truth state had a significant spatial gradient in one parameter: we varied τ_{si} , which essentially scales the slow inward current, between 28.7 and 29.3 spatially following a sinusoidal pattern, as shown in Fig. 10. The truth state shows more pronounced variations in wavelength than when τ_{si} is set to 29 uniformly throughout the tissue (as in the truth state in Fig. 1, for example). After an additional period of adjustment in which resting membrane potential is difficult to achieve, which is found even without spatial heterogeneity, the algorithm is able to match the wavelength and reconstruct the truth fairly accurately, even though it is ignorant of the intrinsic heterogeneity in the truth state. Note that some slight oscillations in the wave shape remain, as can be seen in the wave profile at 1400 ms. The RMS error values fall below the level of the noise in the observations within two rotations of the wave around the ring and remain small for the rest of the simulation. Thus, this preliminary result suggests that data assimilation may perform well even when the numerical prediction model does not describe spatial heterogeneity of the truth state.

IV. DISCUSSION

In this paper, we have considered how the data assimilation algorithm we described previously works with a variety of model error scenarios. To assess the level of error present

in the reconstructed state estimates, we used synthetic observations generated from a spatiotemporal subsampling of a single variable of a known model-generated truth state. While keeping the numerical prediction model used within the LETKF algorithm unchanged, we varied the truth state used over a broad range of dynamical conditions generated by using the same model for prediction but with one or more model parameters changed, by using a different model entirely, and by introducing spatial heterogeneity. We found that including multiplicative inflation to increase the estimate of the ensemble covariance, which increased the uncertainty of the numerical model prediction, was useful for allowing the LETKF to weight the observations more heavily, thereby preventing ensemble collapse. We also found that using additive inflation resulted in further improvement because of its ability to add new directions to the ensemble, which is important when the ensemble and error subspaces differ. By including these inflation factors, in nearly every case, the model performed well and recovered the truth state voltage at high spatial and temporal resolution along with the unobserved model variables with a level of error at or below the level of noise added to the observations.

A. Aspects of data assimilation performance with model error

1. Acceptable range of differences in model dynamics

We tested how well a numerical prediction model tuned to produce a discordant alternans state on its own could adapt to very different types of dynamics in the truth state. We found that the model could successfully match truth states with and without alternans, stronger and weaker alternans, longer and shorter wavelengths, and faster and slower propagation speeds. The main difficulties we observed were slightly higher error for vastly shorter wavelengths (e.g., for

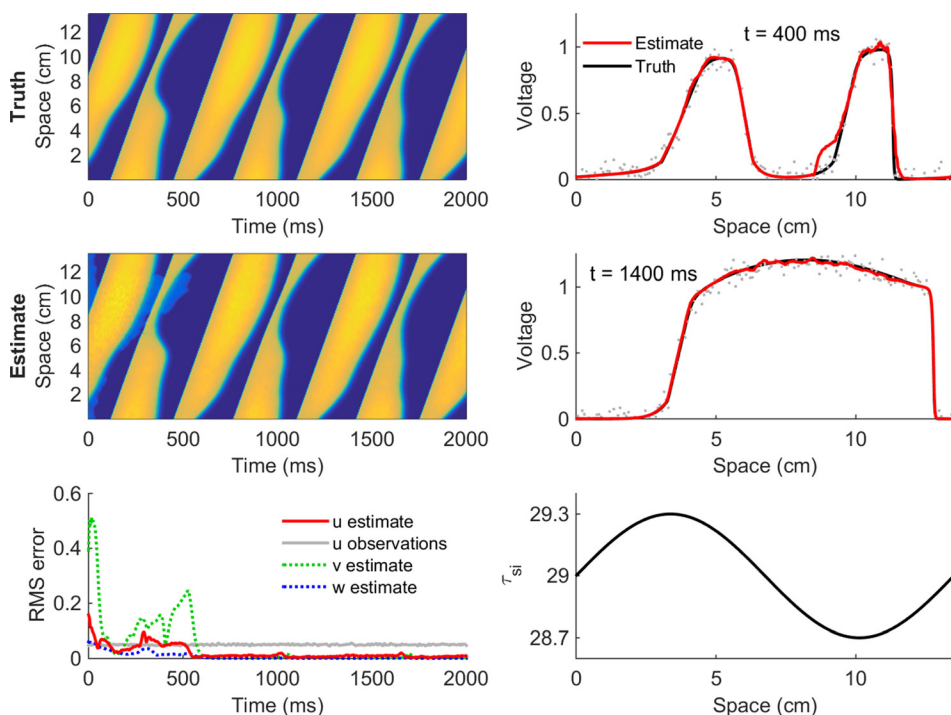


FIG. 10. Effectiveness of the LETKF in the presence of spatial heterogeneity in the truth state in the form of a sinusoidal variation in τ_{si} between 28.7 and 29.3. Very good agreement is obtained. Gray dots in the wave profiles indicate the synthetic observations.

wavelengths under 3 cm when the numerical prediction model generated oscillating wavelengths of around 4–12 cm), for large differences in wave speed (e.g., slower by 50%), and for action potential shapes that differed significantly between the truth and prediction model (e.g., BR action potential vs. FK model action potential shape). For the unobserved variables, when the wave speed is incorrect the errors in the gating variable v can be higher than the errors in the voltage, whereas errors in the gating variable w typically are quite low. However, even for the most challenging conditions, data assimilation still gave reasonable results with errors that did not grow over time. The worst case was for the “Alt GP” parameter set (see Fig. 8), for which RMS error was up to about 7 times higher than the observation noise level. Still, even in this case, for which the truth state had much faster propagation and substantially shorter wavelengths than the prediction model, the overall dynamics of the estimate largely agreed with the truth—there were no vastly different wavelengths, no wave breaks, and no long-term growth trend in the error. Thus, even for the worst case, many important dynamical features were captured correctly.

Overall, our main findings in this regard are (i) data assimilation can be used successfully to produce reconstructions of truth states close to a wide variety of dynamical states, not only dynamics close to the intrinsic dynamics of the numerical prediction model; (ii) roughly, but not necessarily exactly, matching the wave speed in the numerical prediction model to the speed in the truth may be important for obtaining more accurate estimates; (iii) roughly, but not exactly matching the wavelengths may increase accuracy; (iv) inflation helps to check error growth.

2. Why resting membrane potential is initially difficult for the algorithm to achieve

A common problem experienced early in the data-assimilation process is difficulty in reaching resting membrane potential in the wake of a wave. Typically, this behavior ceases within about two rotations of the wave around the ring. The reason for the elevated membrane potential is that at each assimilation time the state estimate from the prediction model is obtained by averaging the voltages of the ensemble members. Having even a single ensemble member with a reasonable wave front location but a wavelength that is too long means that, upon averaging, the membrane potential is elevated just behind the wave. Over a short period of time, the ensemble states improve so that there is better agreement with the location of the wave back. When this has occurred, the membrane potential behind the wave reaches resting potential. We found that this agreement typically occurred within two rotations of the wave—that is, the effects of initialization were noticeable for the first rotation, as expected, and for one additional rotation, but largely disappeared after that.

3. Effect of stochasticity in initialization of the ensemble

Figure 2 shows several examples of reconstructed state estimates obtained using different sets of random model

states to initialize the ensemble members. In the absence of inflation ($m = 1$, $a = 0$), as shown in the upper rows of Fig. 2, the effects of the initialization are clear and can persist. For example, in two of the cases shown, there is a wave break; for one of these cases, the break heals very quickly, but for the other, the break lasts long enough that when the wave becomes reestablished through assimilation of the observations, the wave briefly is able to propagate bidirectionally. Apart from these transient qualitatively different dynamics, the magnitudes and locations of error (see Figs. 1 and 2) can vary. However, using inflation typically mitigates these types of errors. For example, setting $m = 1.2$ for the same case decreases error significantly (see Figs. 1 and 2). For all the remaining cases shown, transient wave breaks and unchecked error growth are prevented (with the possible exception of the case with $\tau_d = 0.24$, $\tau_r = 33$ in Fig. 7, which shows a very short-lived wave break) when both multiplicative inflation and additive inflation are used.

4. How the use of inflation improves state estimates

We showed here that multiplicative and additive inflation can help to improve the accuracy of reconstructed states. One important role that inflation can play is to reduce the likelihood and impact of ensemble collapse, a phenomenon in which the ensemble members converge to nearly identical states, so that the LETKF has a high degree of confidence in the numerical model prediction and pays less attention to the observations during assimilation. Because of the small number of ensemble members, the ensemble sample covariance is often artificially low. Multiplicative inflation helps by increasing the covariance, which leads to increased uncertainty in the numerical prediction and more weight placed on the observations when calculating an improved state estimate. Using additive inflation provides additional help by allowing perturbations to the ensemble members that are not within the error subspace, thereby allowing the ensemble to explore different directions not already present. This procedure can allow the ensemble to span different dynamical states, which can lead to better, typically higher, estimates of uncertainty that again force the LETKF to weight the observations more heavily during assimilation. Overall, inflation helps to prevent overconfidence in the numerical prediction that arises because of agreement among a relatively small number of ensemble members.

B. Limitations

Our findings suggest that model error may not be a significant problem for reconstructing cardiac wave dynamics using data assimilation, even when the dynamics of the numerical prediction model are substantially different from those of the truth. Of course, it is likely that the best results will be obtained when the prediction model is calibrated to match the wave speeds and wavelengths of the truth, but for the broad range of cases considered here the LETKF is robust enough to be effective even when model error is fairly large.

A significant limitation of our work is that we have not tested the effects of model error in two and three spatial

dimensions in the presence of more complex dynamical states involving one or more rotating waves. It is possible that better model agreement will be more important for data assimilation to work well under such conditions. We also have used the same model for prediction in all cases; other models may show greater sensitivity. We have considered here only a single spatial and temporal resolution for the observations; although we showed previously¹³ that using coarser spatial and temporal resolution slightly prolonged the time required to obtain good reconstructions, these resolutions could be more important here. We also could find different results for different levels of Gaussian error as well as for different spatial distributions of observations. Furthermore, the results we showed here included only a single set of parameter values for the prediction model while varying the truth state. It is possible that some sets of parameter values allow more robust state reconstruction than others. In addition, we tested only a single preliminary state with spatial heterogeneity and need to do more work studying this case before we can draw broader conclusions regarding how successful the LETKF is for different heterogeneity shapes, different parameter values, and different ranges of parameter values used over space. Finally, we also have not tested how well the model will perform with experimental data.

C. Future work

Our next steps involve addressing some of the limitations of the present study. We intend to analyze different spatial distributions of observations as well as more complex two- and three-dimensional states, including spiral/spiral wave breakup. We also plan to work with experimental data, which will require understanding more realistic ways to represent heterogeneous, anisotropic tissue with variable shape and thickness. Finally, we are also studying the use of parameter estimation, including spatially varying parameters, within the context of data assimilation.

ACKNOWLEDGMENTS

This work is supported in part by the National Science Foundation under Grant Nos. CMMI-1234235 and CNS-1446312. This work was conducted as a part of the Prediction and Control of Cardiac Alternans Working Group at the National Institute for Mathematical and Biological Synthesis, sponsored by the National Science Foundation through NSF Award No. DBI-1300426, with additional support from The University of Tennessee, Knoxville.

APPENDIX A: DATA ASSIMILATION ALGORITHM

The data assimilation algorithm we use is the Local Ensemble Transform Kalman Filter,¹⁴ which is a nonlinear extension to the Kalman filter. An improved state estimate, called the analysis x^a , is sought by combining the background state estimate x^b with observations y^o to minimize error variance. A small number (here $k = 20$) of ensemble members, each denoted as $x^{b(i)}$, is used to characterize the background forecast covariance. At each assimilation time, the background state estimate is found as the ensemble mean

$$x^b = \frac{1}{k} \sum_{i=1}^k x^{b(i)},$$

and the background covariance is calculated as the ensemble sample covariance

$$\mathbf{P}^b = \frac{1}{k-1} \sum_{i=1}^k (x^{b(i)} - x^b)(x^{b(i)} - x^b)^T.$$

Observations are assumed to include Gaussian errors expressed as the truth plus a Gaussian random variable ϵ , with associated covariance matrix \mathbf{R} . Because the observations are sparse in space, the matrix H is used to map from m -dimensional model space to l -dimensional observation space, so that the observations can be expressed as $y^o = H(x^t) + \epsilon$, where x^t is the true state.

The LETKF solves for the minimizer x of the cost function

$$J(x) = (x - x^b)^T \mathbf{P}^{b-1} (x - x^b) + [y^o - H(x)]^T \mathbf{R}^{-1} [y^o - H(x)].$$

A closed-form solution for the minimizer, which will be the new analysis mean (and thus the improved state estimate), is given by

$$\mathbf{x}^a = \mathbf{x}^b + \mathbf{X}^b \tilde{\mathbf{P}}^a \mathbf{Y}^{bT} \mathbf{R}^{-1} (\mathbf{y}^o - \mathbf{y}^b),$$

where \mathbf{X}^b is the $m \times k$ matrix whose i th column is $x^{b(i)} - x^b$ and \mathbf{Y}^b is the $l \times k$ matrix whose columns are the background ensemble perturbations in observation space. In addition, the analysis error covariance in ensemble space is specified as $\tilde{\mathbf{P}}^a = [(k-1)\mathbf{I} + \mathbf{Y}^{bT} \mathbf{R}^{-1} \mathbf{Y}^b]^{-1}$. The updated ensemble members are generated by adding to the analysis mean the perturbations given by $\mathbf{X}^a = \mathbf{X}^b [(k-1)\tilde{\mathbf{P}}^a]^{1/2}$.

The use of multiplicative inflation modifies the covariance through inclusion of a multiplicative factor m (here it is divided because an inverse is taken): $\tilde{\mathbf{P}}^a = [m^{-1}(k-1)\mathbf{I} + \mathbf{Y}^{bT} \mathbf{R}^{-1} \mathbf{Y}^b]^{-1}$. Additive inflation involves an additional term when generating updated ensemble members: specifically, a multiple a of a vector z is added to the analysis mean plus the perturbations. Here, z is a randomly chosen difference between states spaced 5 ms apart (the assimilation interval) in the spinup.

Further information about the LETKF and our previous application of it to cardiac electrical dynamics can be found in Refs. 14 and 13, respectively.

APPENDIX B: NUMERICAL PREDICTION MODEL

For the numerical prediction model, we use a monodomain formulation of cardiac tissue with the Fenton-Karma (FK) model. The FK model includes one differential equation for the membrane potential u and two others for the gating variables v and w

$$\partial_t u(t, \mathbf{x}) = D \nabla^2 u - I_{ion}(u, v, w),$$

$$\frac{\partial v(t, \mathbf{x})}{\partial t} = \begin{cases} -\frac{v}{\tau_v^+}, & u \geq u_c \\ \frac{1-v}{\tau_{v1}^-}, & u_c > u \geq u_v \\ \frac{1-v}{\tau_{v2}^-}, & u < u_v, \end{cases}$$

$$\frac{\partial w(t, \mathbf{x})}{\partial t} = \begin{cases} -\frac{w}{\tau_w^+}, & u \geq u_c \\ \frac{1-w}{\tau_w^-}, & u < u_c. \end{cases}$$

Periodic boundary conditions are used to form a ring, and the diffusion coefficient D is set to $0.001 \text{ cm}^2/\text{ms}$. The term $I_{ion} = I_{fi} + I_{si} + I_{so}$ is defined as the sum of the fast inward current I_{fi} , the slow outward current I_{so} , and the slow inward current I_{si} , which represent the sodium, potassium, and calcium currents, respectively.

$$I_{fi} = \begin{cases} -\frac{(1-u)(u-u_c)v}{\tau_d}, & u \geq u_c \\ 0, & u < u_c, \end{cases}$$

$$I_{so} = \begin{cases} \frac{1}{\tau_r}, & u \geq u_c \\ \frac{u}{\tau_o}, & u < u_c, \end{cases}$$

$$I_{si} = -\frac{w}{2\tau_{si}} (1 + \tanh(k(u - u_c^{si}))).$$

Except where noted otherwise, we also use the FK model to generate truth states. The variables u , v , and w are initialized to 0, 1, and 0.7, respectively; setting $w = 0.7$ decreases the wavelength of the first wave generated and thereby facilitates the development of discordant alternans within the chosen ring size. To generate the spinup and truth state, a rotating wave is initiated by initially setting u to 1 for the first 0.25 cm of the cable with no-flux boundary conditions; after 200 ms, the boundary conditions are switched to periodic to

TABLE I. Parameter values used for the FK model. The BR and Traj parameter sets correspond to Sets 3 and 1, respectively, from Ref. 6; the Alt GP set is based on the GP parameter set from Ref. 28.

Parameter	BR set	Traj set	Alt Traj set	Alt GP set	Fast Alt GP set
τ_v^+	3.33	3.33	3.33	8.7	8.7
τ_{v1}^-	19.6	19.6	19.6	40	40
τ_{v2}^-	1250	1000	1000	333	333
τ_w^+	870	667	1200	1000	1000
τ_w^-	41	11	50	65	65
τ_d	0.25	0.25	0.25	0.11494	0.22988
τ_o	12.5	8.3	8.3	12.5	12.5
τ_r	33.33	50	50	25	25
τ_{si}	29	45	45	22	22
k	10	10	10	10	10
u_c^{si}	0.85	0.85	0.85	0.85	0.85
u_c	0.13	0.13	0.13	0.13	0.13
u_v	0.04	0.055	0.055	0.025	0.025

allow the wave to propagate indefinitely with no further intervention. For the numerical prediction model, the randomly drawn states from the spinup are used as initial conditions, and only the ring geometry is used.

Table I shows the parameter values used throughout the manuscript. Unless noted otherwise, the BR parameter set is used.

¹E. M. Cherry and F. H. Fenton, *New J. Phys.* **10**, 125016 (2008).
²F. X. Witkowski, L. J. Leon, P. A. Penkoske, W. R. Giles, M. L. Spano, W. L. Ditto, and A. T. Winfree, *Nature* **392**, 78 (1998).
³R. A. Gray, J. Jalife, A. Panfilov, W. T. Baxter, C. Cabo, J. M. Davidenko, and A. M. Pertsov, *Circulation* **91**, 2454 (1995).
⁴J. M. Davidenko, A. V. Pertsov, R. Salomonsz, W. Baxter, and J. Jalife, *Nature* **355**, 349 (1992).
⁵R. A. Gray, A. M. Pertsov, and J. Jalife, *Nature* **392**, 75 (1998).
⁶F. H. Fenton, E. M. Cherry, H. M. Hastings, and S. J. Evans, *Chaos* **12**, 852 (2002).
⁷M. A. Watanabe, F. H. Fenton, S. J. Evans, H. M. Hastings, and A. Karma, *J. Cardiovasc. Electrophysiol.* **12**, 196 (2001).
⁸Z. Qu, A. Garfinkel, P. S. Chen, and J. N. Weiss, *Circulation* **102**, 1664 (2000).
⁹J. J. Fox, M. L. Riccio, F. Hua, E. Bodenschatz, and R. F. Gilmour, Jr., *Circ. Res.* **90**, 289 (2002).
¹⁰G. Salama, in *Optical Mapping of Cardiac Excitation and Arrhythmias*, edited by D. S. Rosenbaum and J. Jalife (Futura Publishing Co., Armonk, NY, 2001), pp. 9–31.
¹¹R. Arora, M. K. Das, D. P. Zipes, and J. Wu, *Indian Pacing Electrophysiol. J.* **3**, 187 (2003).
¹²I. R. Efimov, V. P. Nikolski, and G. Salama, *Circ. Res.* **95**, 21 (2004).
¹³M. J. Hoffman, N. S. LaVigne, S. T. Scorse, F. H. Fenton, and E. M. Cherry, *Chaos* **26**, 013107 (2016).
¹⁴B. R. Hunt, E. J. Kostelich, and I. Szunyogh, *Physica D* **230**, 112 (2007).
¹⁵I. Szunyogh, E. J. Kostelich, G. Gyarmati, D. J. Patil, B. R. Hunt, E. Kalnay, E. Ott, and J. A. Yorke, *Tellus A* **57**, 528 (2005).
¹⁶I. Szunyogh, E. J. Kostelich, G. Gyarmati, E. Kalnay, B. R. Hunt, E. Ott, E. Satterfield, and J. A. Yorke, *Tellus A* **60**, 113 (2008).
¹⁷M. J. Hoffman, S. J. Greybush, R. John Wilson, G. Gyarmati, R. N. Hoffman, E. Kalnay, K. Ide, E. J. Kostelich, T. Miyoshi, and I. Szunyogh, *Icarus* **209**, 470 (2010).
¹⁸T. M. Hamill and J. S. Whitaker, *Mon. Weather Rev.* **133**, 3132 (2005).
¹⁹J. S. Whitaker, T. M. Hamill, X. Wei, Y. Song, and Z. Toth, *Mon. Weather Rev.* **136**, 463 (2008).
²⁰M. J. Hoffman, T. Miyoshi, T. Haine, K. Ide, R. Murtugudde, and C. W. Brown, *J. Atmos. Oceanic Technol.* **29**, 1542 (2012).
²¹L. M. Munoz and N. F. Otani, in *Computing in Cardiology Conference (CinC)*, 2013 (2013), pp. 53–56.
²²A. Garzón, R. O. Grigoriev, and F. H. Fenton, *Phys. Rev. E* **84**, 041927 (2011).
²³S. Berg, S. Luther, and U. Parlitz, *Chaos* **21**, 033104 (2011).
²⁴G. Ullah and S. J. Schiff, *PLoS Comput. Biol.* **6**, e1000776 (2010).
²⁵F. Hamilton, T. Berry, N. Peixoto, and T. Sauer, *Phys. Rev. E* **88**, 052715 (2013).
²⁶E. J. Kostelich, Y. Kuang, J. M. McDaniel, N. Z. Moore, N. L. Martirosyan, and M. C. Preul, *Biol. Direct* **6**, 64 (2011).
²⁷A. Gizzi, E. M. Cherry, S. Luther, and F. H. Fenton, *Front. Physiol.* **4**, 71 (2013).
²⁸F. Fenton and A. Karma, *Chaos* **8**, 20 (1998).
²⁹A. Bueno-Orovio, E. M. Cherry, and F. H. Fenton, *J. Theor. Biol.* **253**, 544 (2008).
³⁰E. M. Cherry, J. R. Ehrlich, S. Nattel, and F. H. Fenton, *Heart Rhythm* **4**, 1553 (2007).
³¹R. A. Oliver and W. Krassowska, *Ann. Biomed. Eng.* **33**, 907 (2005).
³²A. Bueno-Orovio, E. M. Cherry, S. J. Evans, and F. H. Fenton, *BioMed Res. Int.* **2015**, e197586.
³³G. W. Beeler and H. Reuter, *J. Physiol. (London)* **268**, 177 (1977).
³⁴I. Cohen, W. Giles, and D. Noble, *Nature* **262**, 657 (1976).
³⁵D. Di Bernardo and A. Murray, *Nature* **403**, 40 (2000).
³⁶C. Antzelevitch and J. Fish, *Basic Res. Cardiol.* **96**, 517 (2001).
³⁷F. G. Akar and D. S. Rosenbaum, *Circ. Res.* **93**, 638 (2003).
³⁸A. V. Glukhov, V. V. Fedorov, Q. Lou, V. K. Ravikumar, P. W. Kalish, R. B. Schuessler, N. Moazami, and I. R. Efimov, *Circ. Res.* **106**, 981 (2010).